Since January 2020 Elsevier has created a COVID-19 resource centre with free information in English and Mandarin on the novel coronavirus COVID-19. The COVID-19 resource centre is hosted on Elsevier Connect, the company's public news and information website.

Elsevier hereby grants permission to make all its COVID-19-related research that is available on the COVID-19 resource centre - including this research content - immediately available in PubMed Central and other publicly funded repositories, such as the WHO COVID database with rights for unrestricted research re-use and analyses in any form or by any means with acknowledgement of the original source. These permissions are granted for free by Elsevier for as long as the COVID-19 resource centre remains active.

Bioorg. Med. Chem. Lett. 43 (2021) 128079

Contents lists available at ScienceDirect

Bioorganic & Medicinal Chemistry Letters

journal homepage: www.elsevier.com/locate/bmcl

Exploring the potential of novel phenolic compounds as potential therapeutic candidates against SARS-CoV-2, using quantum chemistry, molecular docking and dynamic studies

Maimoona Zia [a], Shabbir Muhammad [b], Shafiq-urRehman [a,*], Shamsa Bibi [a,*], Sumra Wajid Abbasi [c], Abdullah G. Al-Sehemi [f], Aijaz Rasool Chaudhary [d], Fu Quan Bai [e]

[a] Department of Chemistry, University of Agriculture Faisalabad, Faisalabad 38000, Pakistan
[b] Department of Physics, College of Science, King Khalid University, Abha 61413, P.O. Box 9004, Saudi Arabia
[c] Department of Biological Sciences, National University of Medical Sciences, Rawalpindi 46000, Pakistan
[d] Department of Physics, Collehge of Science, University of Bisha, Bisha 61922, P.O. Box 551, Saudi Arabia
[e] Institute of Theoretical Chemistry and College of Chemistry, Jilin University, Changchun 130023, China
[f] Department of Chemistry, College of Science, King Khalid University, Abha 61413, P.O. Box 9004, Saudi Arabia

ARTICLE INFO

Keywords:
SARS-CoV-2
Phenolic compounds
Molecular docking
Molecular dynamics
ADMET

ABSTRACT

In the current study, the interaction of SARS-CoV-2 protein (A and B chains of nsp13) with different recently synthesized phenolic compounds (Sreenivasulu et al., Synthetic Communications, 2020, 112–122) has been studied. The interactions have been investigated by using molecular docking, quantum chemical and molecular dynamics simulations methods. The molecular structures of all the ligands are studied quantum chemically in terms of their optimized structures, 3-D orbital distributions, global chemical descriptors, molecular electrostatic potential plots and HOMO-LUMO orbital energies. All the ligands show reasonably good binding affinities with nsp-13 protein. The ligand L2 shows to have better binding affinities to Chain A and Chain B of nsp13 protein, which are −6.7 and −6.4 kcal/mol. The study of intermolecular interactions indicates that L2 shows different hydrophobic and hydrogen bond interactions with both chains. Furthermore, molecular dynamic simulations of the nsp13-L2 complex are obtained over a time scale of 60 ns, which indicates its stability and flexibility behavior as assessed in terms of its RMSD and RMSF graphs. The ADMET analysis also shows no violation of Lipinski rule (RO5) by studied phenolic compounds. We believe that the current findings will be further confirmed by in vitro and in vivo studies of these recent phenolic compounds for their potential as inhibitors for SARS-Co-V-2 virus.

Introduction

In December 2019, a new human pathogenic outbreak occurred in Wuhan, China. Lately, it has been recognized as Severe Acute Respiratory Syndrome Coronavirus 2 (SARS-CoV-2). The human-to-human transmission of this virus is possible and was first reported on 22-January-2020. SARS-CoV-2 is spreading speedily worldwide[1] and is now becoming an alarming situation around the globe. It is an urgent need of the hour to explore an effective drug against this virus to ensure the safety of precious human lives. This pandemic is increasing day by day because of no effect of the approved drug is available to combat it. Almost 130 million people have been infected with this outbreak and more than 3 million deaths have been reported on the dashboard of World Health Organization (WHO) till 3rd March, 2021.[2] The typical sign and symptom of an infected person with SARS-CoV-2 is pneumonia. Besides, dyspnea or shortness of breath, cough, headache, fatigue, chest pain, muscle ache, diarrhea, fever, sore throat, anorexia, confusion, vomiting, and nausea have also been observed. At least, four inclusive studies have been executed on clinical and epidemiological features of SARS-CoV-2 infected patients. According to this study, fatigue, cough, and fever were complained by 96%, 68%, and 90% of patients, respectively.[3] Its origin is a bat, which can spread to humans through sneezing, coughing droplets, or direct contact.[4] It can spread up to a distance of one meter through sneezing, water droplets, it builds a principle of maintaining a distance of a meter that is termed as “social distancing”.[5]

Coronavirus belongs to a family *Coronaviridae,* order *Nidovirales*.

* Corresponding authors.
E-mail addresses: shafiq.urrehman@uaf.edu.pk (Shafiq-urRehman), shamsa.shafiq@uaf.edu.pk (S. Bibi).

https://doi.org/10.1016/j.bmcl.2021.128079
Received 17 March 2021; Received in revised form 26 April 2021; Accepted 27 April 2021
Available online 1 May 2021
0960-894X/© 2021 Elsevier Ltd. All rights reserved.

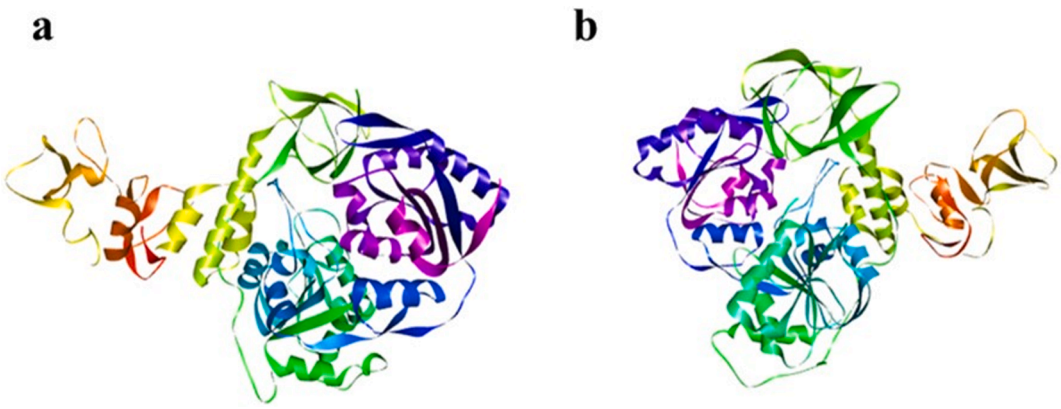

Fig. 1. The 3-D crystal structure of nsp-13 protein of SARS-Co-V-2: (a) Chain A and (b) Chain B.

Coronaviruses are a large family of single-stranded, positive-sense RNA viruses.[6] Like various structural proteins including (M-protease), there are also non-structural proteins that can be used to design/discover a vaccine and drug against SARS-CoV-2. Helicase is a crucial enzyme for viral replication. It can unwind the double-stranded DNA and RNA, and then converts them into two single-stranded nucleic acids. Among the clinically permitted drugs like nucleoside and non-nucleoside reverse transcriptase inhibitor as well as a protease inhibitor and the 3D Structure of SARS-CoV-2 Helicase protein (nsp13) was recognized, certified, and used to monitor its druggable properties.[7] The protein nsp13 plays a significant role in viral replication and transmission in a host. This protein is recognized as one of the most interacting proteins with hosts. Its vibrant role in virus replication as well as its conserved nature makes it a crucial antiviral drug target against SARS-CoV-2.[8] There is a central role of nsp13 in various aspects of the virus life cycle.[9] Keeping in mind the significant function of nsp13 protein, this study is designed to identify helicase inhibitors as probable drugs against nsp13 by using different computational techniques. Computational drug discovery is a speedy and swift way of designing a drug with minimum cost, unlike traditional drug discovery.[10]

For the present work molecular docking study was performed to better understand the binding mechanism of newly synthesized six phenolic compounds as anti-COV2 drugs. The selected six phenolic compounds[11] are named as 2-(1-phenylethyl) phenol as **L1**, 2-methyl-6-(1-phenylethyl) phenol as **L2**, 4,5-dimethyl-2-(1-phenylethyl) phenol as **L3,** 2-chloro-6-(1-phenylethyl) phenol as **L4**, 4-ethyl-2-(1-phenylethyl0 phenol as **L5** and 4-methyl-2-(1-phenylethyl) phenol as **L6.** The optimized structures of all the ligands are documented in Fig. S1 of the supporting information. The phenolic compounds are found in all plant materials naturally and these are secondary plant metabolites. Phenolic compounds are crucial part of human as well as animal diet. These compounds reflect as antioxidant activities to employ anti-microbial, anti-inflammatory, anti-diabetic, anti-allergic, antiviral and vasodilatory effect to inhibit diseases such as cardiovascular illness, eye disorders, cataract, neurodegenerative diseases, cancer and Alzheimer's.[12,13] Phenolic compounds have been gained more attention due to their antioxidant properties, which are very fruitful in the inhibition of several diseases. These compounds indicate a greater ability of catching free radicals to act as antioxidants and playing a vital part in prohibition of several illness including neurodegenerative, cardiovascular and cancer.[14] Phenolic compounds reflect vital therapeutic activity.

Other methodologies are used to discover more efficient therapeutics, including ADMET Analysis, Molecular Electrostatic potential MEP, Frontier Molecular Orbitals (HOMO & LUMO orbitals), and Global Chemical Descriptors (to define the chemical properties of compounds). We expect this study to provide clear insights into the production of the efficient SARS-CoV-2 vaccine/drugs.

Computational details

The molecular docking studies of ligands and the target (SARS-CoV-2 nsp13) are performed by Autodock Vina (ADV)[15] to calculate the binding affinity between ligands and nsp13 protein. The preparation of ligands and protein for molecular docking is done by using MGL Tools. The ligands were kept as flexible with various rotatable bonds while protein (nsp13) macromolecules or substrate were treated as rigid. GAUSSIAN 16 suit of program[16] was used to perform the quantum chemical studies for molecular structural analysis of ligands, while visualization of molecular electrostatic potential and orbitals was accomplished by GaussView5.[17] The chemical structures of the ligands were optimized (the lowest energy conformation) using density functional theory (DFT) method with B3LYP/G* level of theory. The detail of various preparation of docking calculations are given below.

Macromolecule/Protein preparation

To access the 3D structures of biological macromolecules Protein Data Bank (PDB)[18] is the worldwide archive, as it contains efficiently and instantly any information regarding majority of proteins. From PDB (https://www.rcsb.org/), the crystal structure of nsp13 (PDB ID: 6zsl) was retrieved in pdb format (Fig. 1). For protein preparation MGL Tools[19] were used. From macromolecules the co-crystalized ligands and water molecules were removed and polar hydrogens as well as Kollman Charges were added.

Ligands

The 3D structures of ligands were taken from a research paper[11] and to get their optimized structures these were designed on gaussview 05 and then converted into pdb format.

Docking protocol

For molecular docking analysis, pdb files of both protein and ligand were converted in PDBQT format an extended pdb format via MGL tools. Docking analysis performed with grid box sized 80 × 88 × 54 and 1 Å spacing. The output pdbqt files were written into config (configuration) file. The conformation with lowest binding affinity was reflected as most stable ligand conformation with respect to macromolecules. Biovia discovery studio 2020[20] visualizer was used for intermolecular interactions visualizations.

Pharmacokinetics and ADMET study

In pharmaceutical industries, ADMET analysis has a great importance for a productive drug discovery. It provides basis, for the

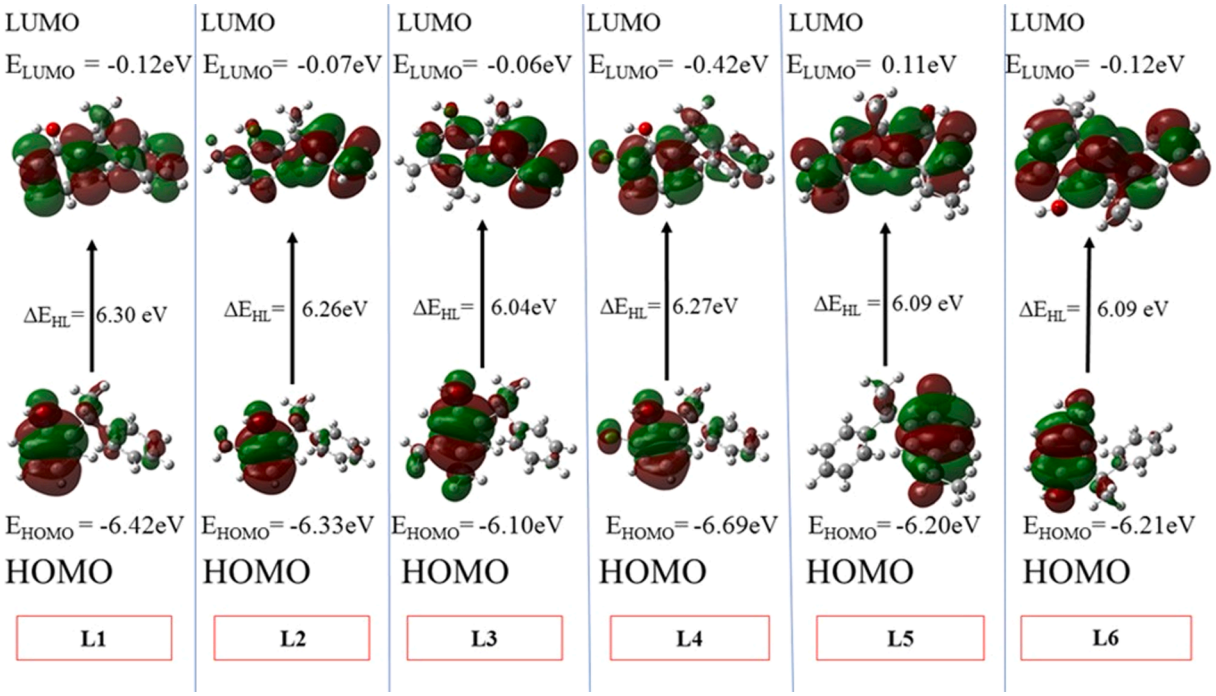

Fig. 2. The 3-D plots of HOMO-LUMO for all studied ligands as calculated at B3LYP/6-311G* level of theory with isovalues of ± 0.002 a.u.

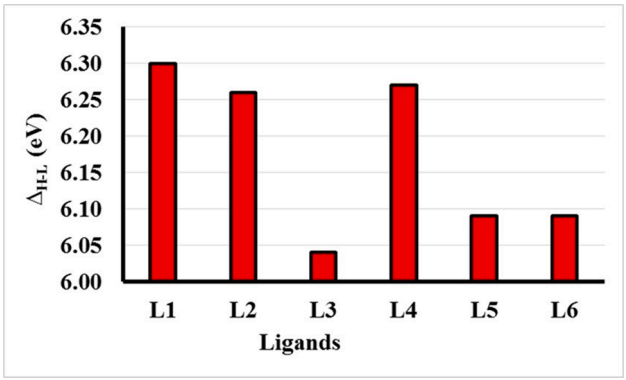

Fig. 3. Comparison of $\Delta_{H\text{-}L}$ energy gap values for all the optimized geometries of ligands calculated at B3LYP/6-311G* method.

successful computational drug and to reduce the undesired effects of a drug. In present study, pharmacokinetic analysis of drugs was performed by using pkCSM[21] an online sever. pkCSM is an open database which provides information regarding drug likeness. The smiles of the ligands are generated in ChemDraw JS online[22] and submitted to pkCSM. The server database run by picking toxicity ADMET module.

Results and discussion

Structural chemistry of ligands

Frontier molecular orbitals and molecular electrostatic potentials

The structural chemistry of ligand can play a crucial role for establishing docking interactions between ligand and protein molecules. The chemical structures and reactivities of ligand molecules are immensely dependent on the distribution patterns and energetics of their frontier molecular orbitals (FMOs). The FMOs usually includes the highest occupied molecular orbital (HOMO) and the lowest unoccupied molecular orbital (LUMO). To shed light on some structural facts, we have optimized the geometries (the lowest energy conformations) of all the compounds using density functional theory method at B3LYP/6-311G* level of theory.[23] The 3-D plots of FMOs and the orbital energies for the optimized geometries of all the compounds were calculated as shown in Fig. 2. A careful analysis of Fig. 2 shows that the HOMOs of all the compounds are somewhat localized on phenol rings only leave no or insignificant electronic density on the other counterpart phenyl ring. In the light of HOMO distributions, it is expected that phenolic ring might show more intermolecular interactions for protein residues as compared to its counterpart phenyl rings. The HOMO energies of all the compounds range from −6.10 eV to −6.42 eV except compound L4 which has −6.69 eV due to the present of halogen atom. Besides, individual energies, the HOMO-LUMO energy gaps ($\Delta E_{H\text{-}L}$) are very crucial for their chemical reactivity[24] and kinetic stability. Generally a lower value of $\Delta E_{H\text{-}L}$ indicates less stability[25] of molecule and its more vulnerability to an attacking nucleophile/electrophile. Based on the $\Delta E_{H\text{-}L}$ values of all the compounds can be arranged in their decreasing $\Delta E_{H\text{-}L}$ values as L1 > L4 > L2 > L5 = L6 > L3. Overall, it is observed from Fig. 3 that the positions of –OH, –CH3 and –Cl groups have significance influence on the orbital energies of all compounds. Fig. 3 illustrates the energy gaps of all ligands. Furthermore, for all compounds, their molecular electrostatic potentials (MEPs) were also calculated on the total density surface of their molecular geometries. The highest negative and positive potentials were characterized by blue and yellow colors[26] while other colors indicate their respective intermediate potentials on the total electron density surface. As shown in Fig. 4, the MEPs not only provide the positive and negative potential regions but also indicates the shape and size differences among the ligands for possible fitting/docking into the protein cavities. The highest negative potentials are seen from the acidic H-atoms of phenolic group, which indicates its potential as favorite moiety for H-bond interactions for docking interactions (Fig 5).

Global chemical descriptors

Global chemical descriptors including Ionization Energy (I), Electron Affinity (A), Chemical Hardness (η), Chemical potential (μ), Electronegativity index (χ), Electrophilicity index (ω) and Softness (S) are important parameters in determining the structure–property relationship of the compounds. Many such electronic structural parameters are used in QSAR studies so we consider it worth to calculate and provide

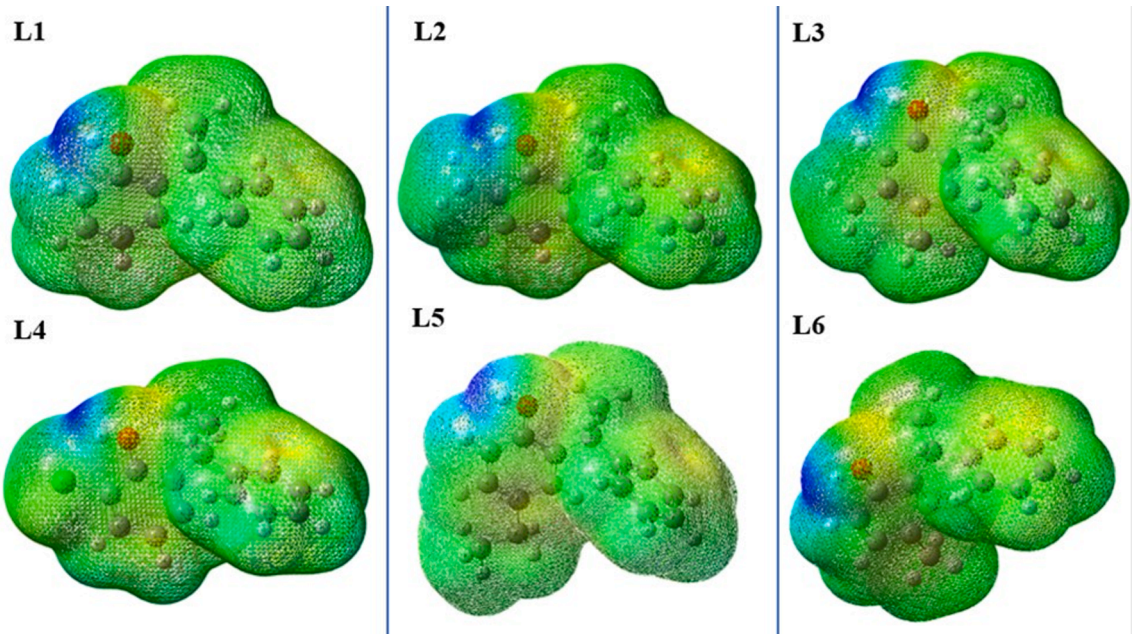

Fig. 4. 3-D plots of MEP (Molecular Electrostatic Potential) for all studied ligands as calculated at B3LYP/6-311G* level of theory with isovalue of ± 0.002 a.u. The blue and yellow color highlights the negative and positive potential of the compounds respectively. While the other colors illustrate their respective intermediate potential on the total electron density surface.

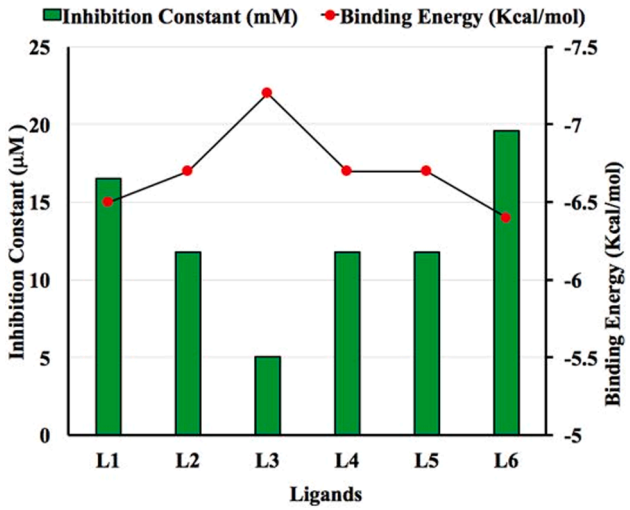

Fig. 5. Comparison between Binding Energy (kcal/mol) and Inhibition Constant (μM) for Chain A of nsp13.

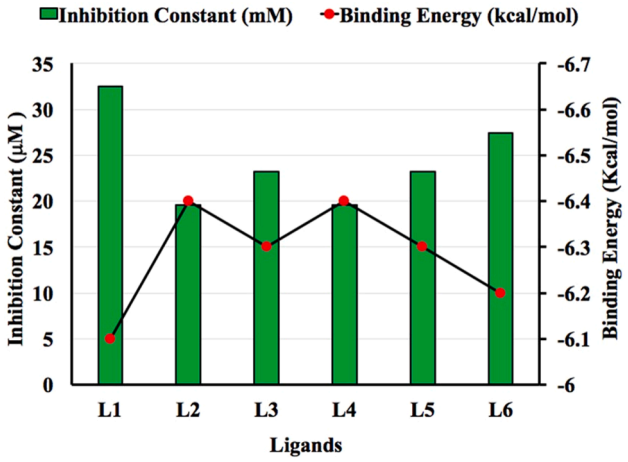

Fig. 6. Comparison between Binding Energy (Kcal/mol) and Inhibition Constant (μM) for Chain B of nsp13.

these parameters as important information for our entitled compounds as given in Table S1 of supporting information. For example, ionization potential which is ease of losing an electron from the valance orbital of a compound also represents the kinetic stability of a compound. The IP values of entitled compounds range from minimum 6.10 eV for compound 3 to maximum 6.69 eV for compound 4 which is typical range for most of the stable organic compounds. Similarly, other global chemical descriptors were also provided and discussed in details in supporting information of the article (see Table S1).

Binding energy and inhibition constant of protein-ligand interactions

Binding energy and binding affinity both have same meanings so we used them interchangeably. It is important to pen down that a more negative binding energy means a better ligand–protein complex while binding affinity is taken as a general term for comparative analysis which is also higher for higher negative values of binding energy. Protein nsp13 consists of two chains A and B. Both chains play a crucial role

Table 1
Molecular docking analysis of different compounds against nsp13 using Auto Dock Vina.

	Protein	*Binding Energy Kcal/mol*	*Inhibition Constant μmol*	*Protein*	*Binding Energy Kcal/mol*	*Inhibition Constant μmol*
Ligands		***Chain A***	***Chain A***		***Chain B***	***Chain B***
L1		−6.5	16.524		−6.1	32.538
L2		−6.7	11.775		−6.4	19.574
L3	**nsp13**	−7.2	5.048	**nsp13**	−6.3	23.188
L4		−6.7	11.775		−6.4	19.574
L5		−6.7	11.775		−6.3	23.188
L6		−6.4	19.574		−6.2	27.468

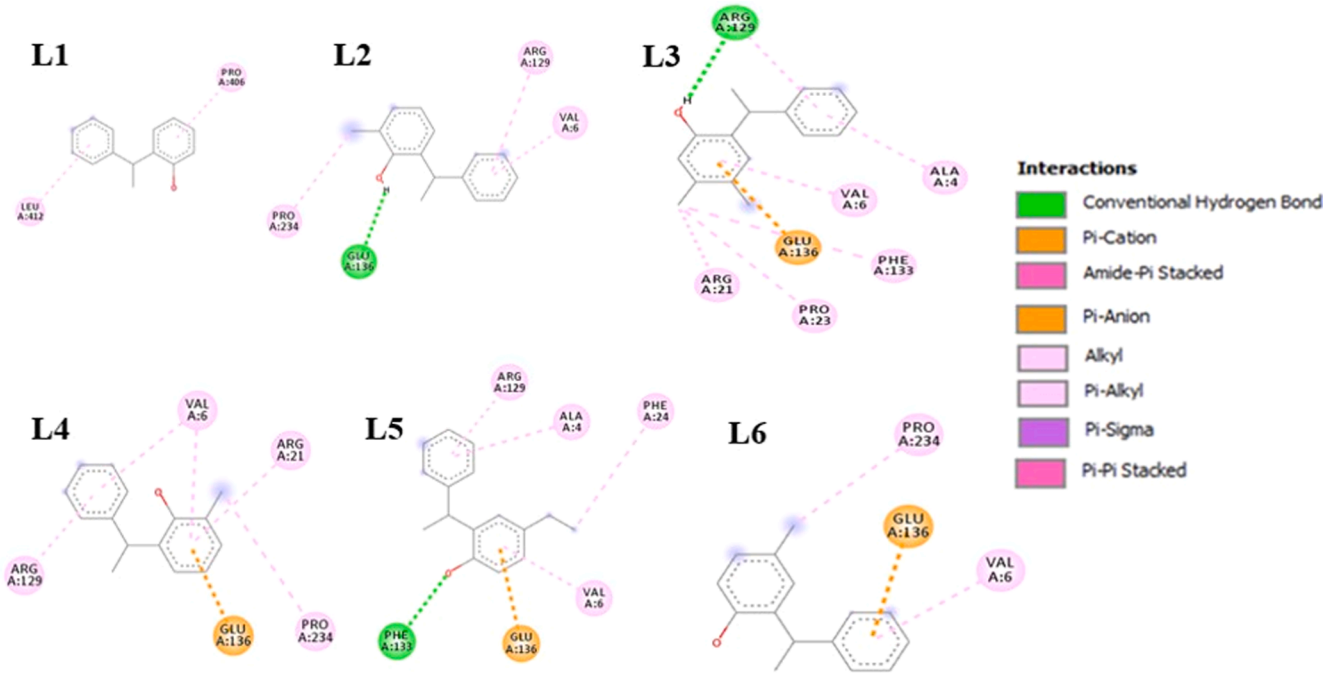

Fig. 7. Ligands (L1, L2, L3, L4, L5 and L6) interactions with Chain A amino acid residues of nsp13.

in binding with ligands. The binding energy values are ranging from −6.4 to −7.2 kcal/mol for Chain A (Fig. 5). The binding energy values for Chain B are ranging from −6.1 to 6.4 kcal/mol (Fig. 6). For Chain A, the inhibition constant values are ranging from 5.048 to 19.574 μmol as well as for Chain B are 19.574 to 32.538 μmol. The binding affinity and inhibition constant of all the ligands for Chain A and B are listed in Table 1. L3 shows the highest binding affinity with Chain A of nsp13 protein of SARS-CoV-2 with binding energy and inhibition constant of −7.2 kcal/mol and 5.048 μmol between all the studied ligands. L2 and L4 show the maximum binding affinity with chain B of nsp13 protein of SARS-CoV-2 with the same binding energy and inhibition constant values of −6.4 kcal/mol and 19.574 μmol among all the planned ligands. However, the results indicate that all ligands disclose the good binding affinity with both chains A and B of nsp13 protein and all these are virtuous potential inhibitors against SARS-CoV-2.For Chain A, order of ligands based on their increasing binding energy is as L6 < L1 < L2 = L4 = L5 < L3. For Chain B, order of ligands based on their increasing binding energy is as L1 < L6 < L3 = L5 < L2 = L4 .

Protein-ligand interactions

The protein nsp13 explores its conserved nature and critical role in viral replication as an ideal antiviral drug target.[27] The nsp13 has a triangular pyramid structure.[28] The enzyme Helicase of coronavirus is a member of superfamily-1 helicase which involving of seven preserved regions. This protein can unwind both duplexes of DNA/RNA. It

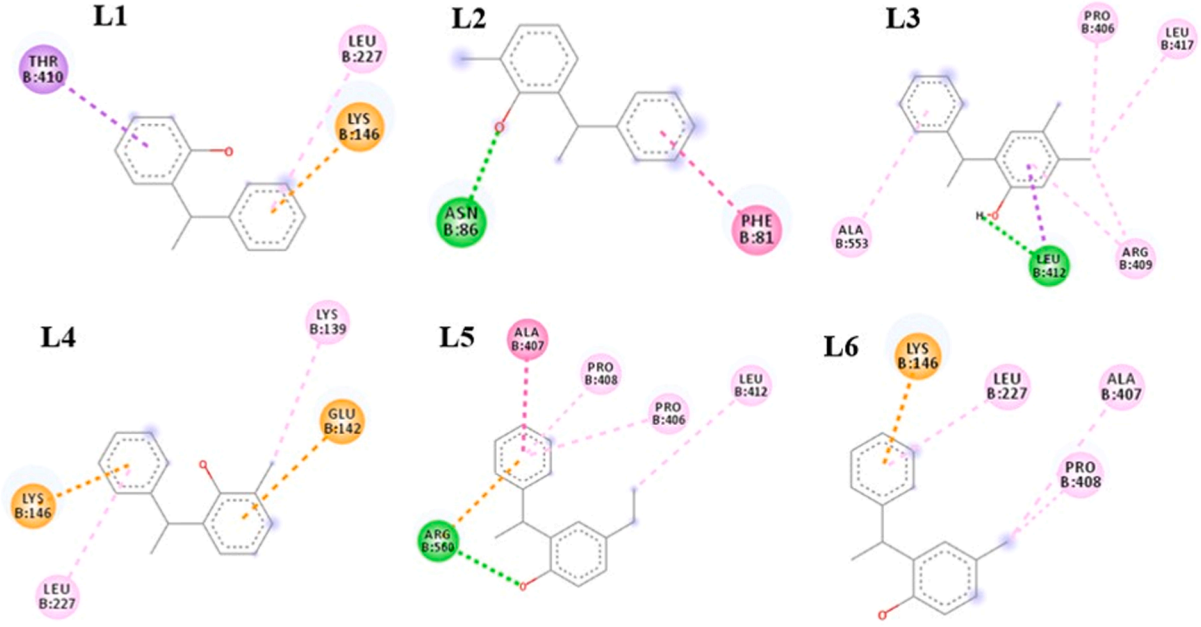

Fig. 8. Ligands (L1, L2, L3, L4, L5, and L6) interactions with Chain B amino acid residues of nsp13.

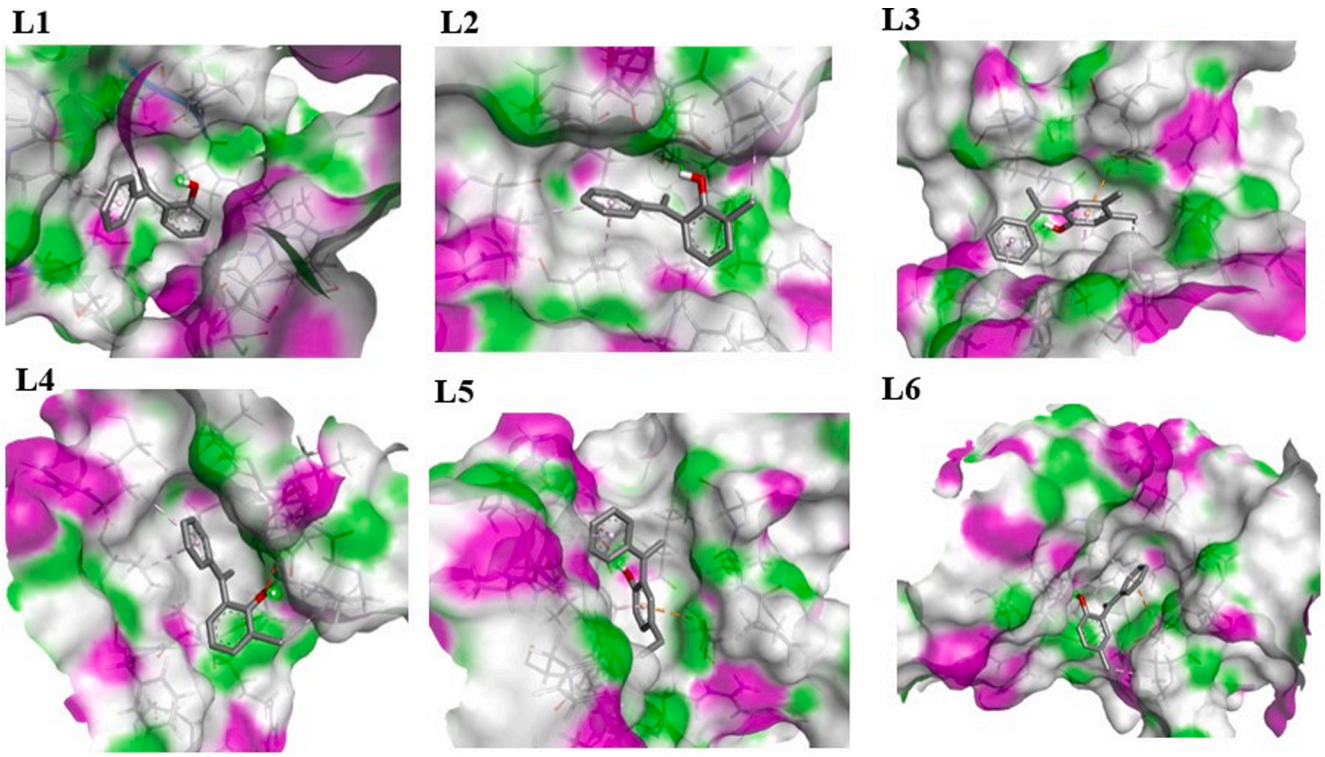

Fig. 9. Hydrogen Bond interactions of ligands (L1, L2, L3, L4, L5 and L6) with Chain A of nsp13, purple color shows H-Bonds donor regions and green for H-Bond acceptors regions.

unwinds the RNA/DNA in 5′-3′ direction.[29] This helicase nsp13 belongs to the SF1 region of six helicase super families. There are several motifs in the SF1 region, those intricate in direct binding with nucleic acid and nucleic acid triphosphates. Two motifs known as Walker motifs such as A and B are common members of this superfamily. This enzyme is tangled in viral RNA synthesis as well as in manipulation of host DNA.[30] All the planned ligands show innovative interactions with different amino acid residues of both chains A and B. The interactions between

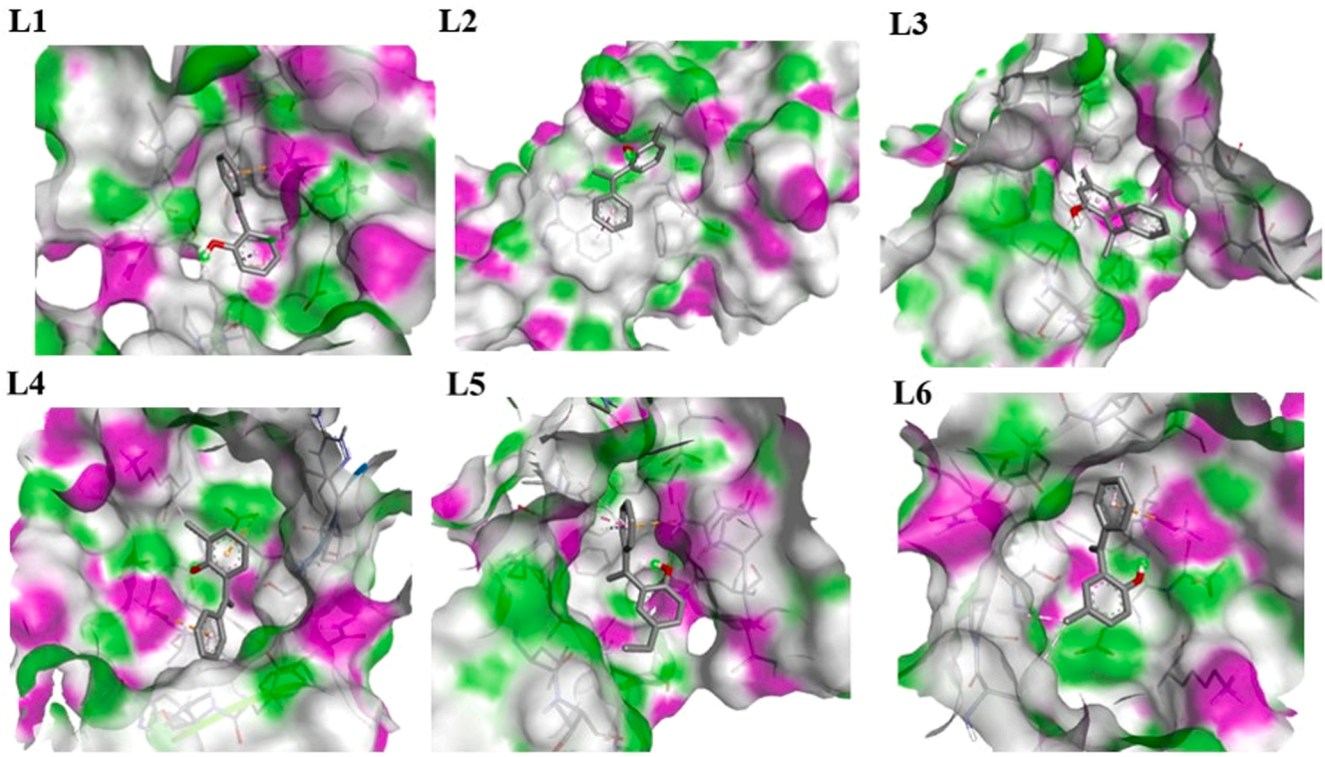

Fig. 10. Hydrogen Bond interactions of ligands (L1, L2, L3, L4, L5, and L6) with Chain B of nsp13, purple color shows H-Bonds donor regions and green for H-Bond acceptors regions.

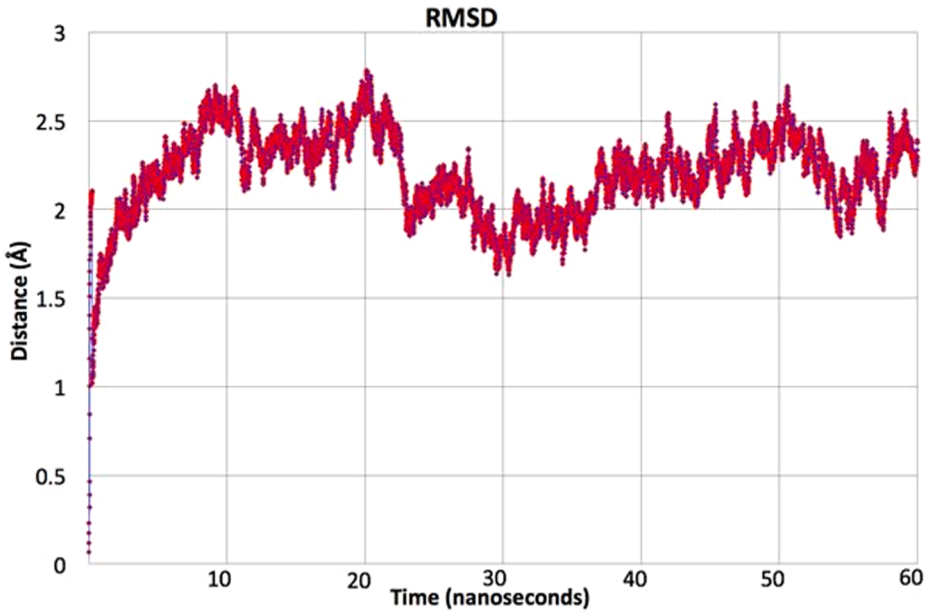

Fig. 11. RMSD graph of L2 with Chain B of nsp13.

macromolecule (protein) and small molecules (ligands) are usually carried out through various acting forces such as van der wall forces, hydrophobic, electrostatic, and hydrogen bond interactions.[31] The hydrophobic interactions are involved in π-alkyl, alkyl, π-amide stacked, π-sigma and π-π stacked interactions. The electrostatic interactions are involved in π-cation and π-anion interactions.

Molecular docking results in different types of interactions of ligands with a different amino acid residue of the protein. Ligands show effective binding with both chains A and B of the protein. All these ligands and protein interactions are visualized by using Discovery Studio Visualizer software.[32] 2D diagrams of DSV shows the binding and interactions of ligands with different amino acid residues of the protein. With Chain A, ligand L1 shows two types of hydrophobic (π-alkyl) interactions with PRO406 and LEU412. L2 shows three types of hydrophobic interactions and one hydrogen interaction with ARG129, VAL6, PRO234, and GLU136, respectively. L3 shows eight types of interactions in which six are hydrophobic π-alkyl and alkyl with ALA4, ARG129, VAL6, PHE133, PRO23, and ARG21, one electrostatic π-anion with GLU136 and one is hydrogen bond interaction with ARG129 as illustrated in Fig. 7. L4 shows six interactions, five are hydrophobic interactions with VAL6, ARG21, PRO234, ARG129, and VAL6, and one is electrostatic π-anion interaction with GLU136. L5 also shows six types of interactions, four are hydrophobic π-alkyl interaction with amino acid residues of ARG129, ALA4, PHE24, and VAL6, one is electrostatic π-anion interaction with GLU136, and one is hydrogen bond interaction with PHE133. L6 shows three types of interactions, two are hydrophobic alkyl and π-alkyl with PRO234, and VAL6, respectively, one electrostatic π-anion interaction with GLU136 Fig. 7.

With Chain B, ligand L1 shows three types of interactions, two are hydrophobic including π-sigma and π-alkyl interaction with THR410 and LEU227, respectively. One is electrostatic pi-cation interaction with LYS146. L2 shows two types of interactions, one is hydrophobic π-π stacked interaction with PHE81 and one is hydrogen bond interaction with ASN86. L3 shows seven types of interactions, six are hydrophobic alkyl (3), π-alkyl (2), and π-sigma (1) interactions with PRO406, LEU417, ARG409, ALA553, ARG409 and LEU412, respectively, while one is hydrogen bond interaction with LEU412 Fig. 8. L4 shows four types of interactions, two are hydrophobic alkyl and π-alkyl interactions with LYS139 and LEU227, respectively. Two are electrostatic π-cation and π-anion interactions with LYS146 and GLU142 respectively. L5 shows six types of interactions, four are hydrophobic alkyl (1), π-alkyl (2), and amide-π-stacked (1) interactions with LEU412, PRO406, PRO408, and ALA407, respectively. One is electrostatic π-cation interaction with ARG560 and one is hydrogen bond interaction with AGR560. L6 shows four types of interactions, three are hydrophobic alkyl (2) and π-alkyl (1) interactions with ALA407, PRO408, and LEU227, respectively. One is electrostatic π-cation interaction with LYS146 Fig. 8. The hydrogen bond interactions of all ligands with Chain A and Chain B are illustrated in Figs. 9 and 10, respectively.

MD simulations

Molecular dynamics are computer simulations that are performed to visualize the physical movement of the protein–ligand complex in aquous environment. For a fixed period of time, protein and ligand are permitted to interact with each other, providing a view of the dynamic evaluation of the system. After completing the molecular docking with a rigid crystal structure of nsp13 protein, the molecular dynamics of the targeted protein Chain B of nsp13 and the best-docked ligand L2 was performed to envisage their dynamic behavior. This selection of Chain B of nsp13 and docked ligand L2 for further dynamic studies is not only based on binding energy but also on visualization of better intermolecular interactions. We performed MD simulations for 60 ns (6 × 106 fs) time scale for the best-docked complex. All calculations of molecular dynamics simulations are performed by using the CHARMM forcefield[33] in NAMD.[34] The details of all input parameters of molecular dynamic are given in supporting information of article. The root mean square deviation (RMSD) and root mean square fluctuation (RMSF) calculations were completed by using the VMD program.[35] To evaluate the thermodynamic stability of the complex during molecular dynamics for 60 ns, RMSD analysis of the complex was done. The RMSD graph of the complex is shown in Fig. 11. Different trends are shown in the RMSD graph of the complex at different time intervals. Overall fluctuations are seen between 1 and 3 Å which is reported in literature.[36] The RMSD of the complex is seems to be equilibrated after 10 ns as moving from 1 to 60 ns via different fluctuations. After 10 ns time interval, the RMSD fluctuations are seen only between 1.5 and 2.7 Å, which are about 1.2 Å of its maximum and minimum amplitude as shown in Fig. 11. This ~ 1.2 Å amplitude further reduced to ~ 0.7 Å amplitude after 38 ns. Different fluctuations are observed at different time intervals i.e. around 11, 20, 30, 43, and 52 ns, which illustrate reasonable flexibility of protein residues and stability of complex containing Chain B of nsp13 and docked

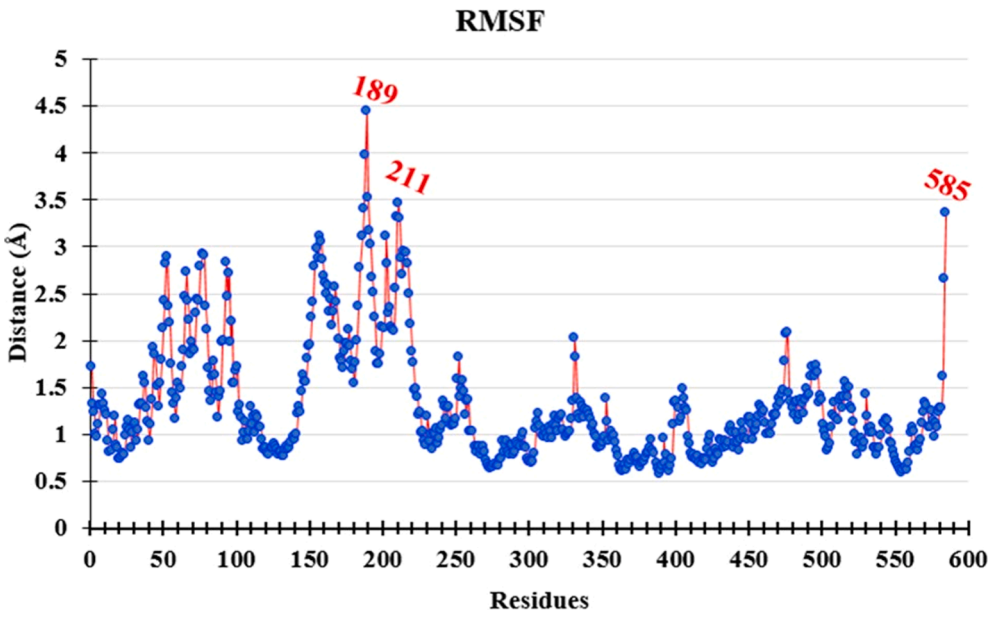

Fig. 12. The root mean square deviation graph of L2-nsp13-B.

Table 2
Absorption, Distribution, Metabolism, and Excretion (ADME) parameters of the Rule of Five for our studied ligands.

ADMET	*Parameters*	*L 1*	*L 2*	*L 3*	*L 4*	*L 5*	*L 6*
Absorption	Water Solubility (log S) (log mol/L)	−3.924	−4.212	−4.528	−4.537	−4.525	−4.150
	Intestinal Absorption %	94.789	94.586	95.494	93.128	94.712	94.413
	p-glycoprotein substrate	No	No	No	No	No	No
	p-glycoprotein I/II Inhibitor	No	No	No	No	No	No
Distribution	VDss (log L/kg)	0.658	0.701	0.791	0.667	0.82	0.635
Metabolism	CYP2D6 Substrate	No	No	No	No	No	No
	CYP3A4 Substrate	Yes	Yes	Yes	Yes	Yes	Yes
	CYP2D6 Inhibitor	No	No	No	No	No	No
	CYP3A4 Inhibitor	No	No	No	No	No	No
Excretion	Total Clearance (Log/ml/min/kg)	0.297	0.307	0.310	0.303	0.335	0.302
	Renal OCT2 substrate	No	No	No	No	No	No
Toxicity	AMES Toxicity	No	No	No	No	No	No
	Max. tolerable dose (log mg/kg/day)	0.615	0.596	0.623	0.586	0.665	0.606
	Hepatotoxicity	No	No	No	No	No	No

ligand L2.[37]

For further thermodynamics conformational stability, the RMSF analysis of the complex are performed. The RMSF graph of the complex is illustrated in Fig. 12. The graph exposed no major fluctuations because there are only 3 residues expressed fluctuations as 4.4, 3.4, and 3.3 Å by 189, 211, and 585 residues, respectively. It is well-known that the last 5 residues usually show higher RMSF values owing to their free ends because at free ends residues are present on the surface of protein.[38] Lowers the fluctuations represent the stability of the complex.[37] It indicates that the complex of the nsp13 protein and L2 ligand is stable (Fig. 12).

ADMET profile

The successful discovery of a drug is based on their drug-likeness and toxicity analysis commonly known as ADMET analysis.[39] These properties play a vital role in the discovery of fruitful drugs. The ADMET properties of the ligands are calculated using the online database pkCSM.[21] To perform the ADMET analysis of studied compounds, smiles are generated by using ChemDraw JS online[22] The smile format of all the ligands is documented in Fig. S2 of the supporting information. All ligands express good ADMET properties. All compounds show good water solubility and effective intestinal absorption. No compound shows any hepatotoxic effect. All these compounds are non-toxic and show the good distribution and excretion properties. L5 has the highest distribution value, and L6 has the lowest distribution value among all studied ligands. L3 has the highest intestinal absorption and L4 has the lowest intestinal absorption. Overall, all compounds show good distribution

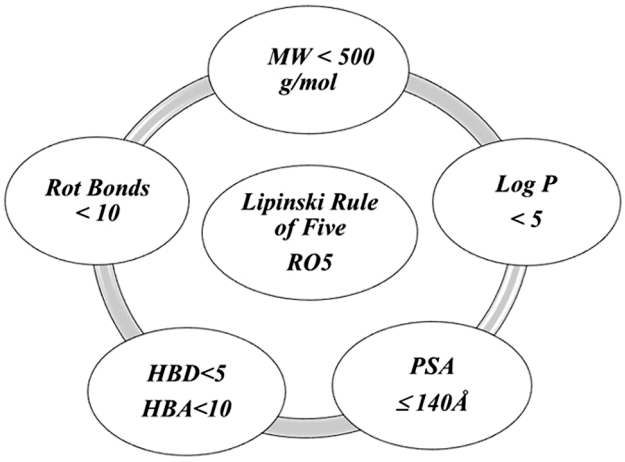

Fig. 13. Lipinski rule of Five (RO5).

values and intestinal absorptions. L5 has the highest maximum tolerable dose value as 0.665 (log mg/kg/day) and L4 has the lowest maximum tolerable dose value as 0.586 (log mg/kg/day). The ADMET properties of all the ligands are listed in Table 2.

Lipinski rule of five (RO5)

RO5 is usually used for drug designing and to predict drug-likeness. All the computational drugs are tested by RO5 (Fig. 13). According to this rule, the molecular weight of a drug should be less than 500 g/mol, polar surface area should be equal and less than 140 Å, log P values should be less than 5, rotatable bonds should be less than 10, Hydrogen Bond donor (HBD) and hydrogen bond acceptor (HBA) should be less than 5 and 10 respectively.[40] All the ligands have a good clearance rate (excretion rate) from the body. L5 and L3 has the highest clearance rate as 0.335 and 0.310 (Log/ml/min/kg) respectively. All studied ligands meet the criteria of RO5 and no compound violates this rule. The Lipinski rule of five of all ligands is calculated by using the pkCSM online database (http://biosig.unimelb.edu.au/pkcsm/prediction). The RO5 analysis of all ligands is documented in Table S2 of supporting information.

Summary

The interaction of SARS-CoV-2 nonstructural protein (nsp13) with different recently synthesized phenol compounds were studied. This study was conducted by using different approaches including molecular docking, quantum chemical, and MD simulations. Unlike earlier studies, firstly, we studied the chemistry of the ligands to explore their reactivity in the form of their optimized structures, 3-D orbital distributions, global chemical descriptors, MEP plots, and HOMO-LUMO orbital energies. The molecular docking of all the ligands accomplished with both chains A and B of nsp13. All the ligands revealed stable complexes with nsp13 targeted protein. Among all the compounds, L2 possessed good binding affinities to Chain A and Chain B of nsp13 protein, which are −6.7 and −6.4 kcal/mol. The MD simulations of L2 complexed with nsp-13 protein were done for 60 ns time scale. The stability and flexibility of docked ligand–protein complex was assessed in terms of its RMSD and RMSF analysis. Moreover, ADMET analysis of all ligands were also performed by the pkCSM online database, which predicted that L2 may has the highest intestinal absorption and total clearance rate. The current study highlights the crucial role of all synthesized ligands for their antiviral activity against SARS-CoV-2. For creating strong experimental evidence, this study further suggests in vitro and in vivo studies of these recent phenolic compounds.

Declaration of Competing Interest

The authors declare that they have no known competing financial interests or personal relationships that could have appeared to influence the work reported in this paper.

Acknowledgements

The author from the University of Bisha extends their appreciation to the Deanship of Scientific Research at the University of Bisha Saudi Arabia for funding this work through COVID-19 Initiative Project under Grant Number (UB - COVID - 32 - 1441). The authors from King Khalid University of Saudi Arabia extend their appreciations to the Deanship of Scientific Research at King Khalid University for funding the work through Project (RGP.1/168/42). For computer time, this research used the resources of the Supercomputing Laboratory at King Abdullah University of Science & Technology (KAUST) in Thuwal, Saudi Arabia.

Appendix A. Supplementary data

Supplementary data to this article can be found online at https://doi.org/10.1016/j.bmcl.2021.128079.

References

[1] Martellucci CA, et al. SARS-CoV-2 pandemic: an overview. *Adv Biol Regul.* 2020;77:100736.
[2] Organization WH. Coronavirus disease (COVID-19). 2020.
[3] Zheng J. SARS-CoV-2: an emerging coronavirus that causes a global threat. *Int J Biol Sci.* 2020;16(10):1678.
[4] Xu G, et al. Clinical pathway for early diagnosis of COVID-19: updates from experience to evidence-based practice. *Clin Rev Allergy Immunol.*. 2020:1–12.
[5] Mishra AK, Tewari SP. In: Silico Screening of Some Naturally Occurring Bioactive Compounds Predicts Potential Inhibitors against SARS-COV-2 (COVID-19) Protease. arXiv preprint arXiv:2004.01634, 2020.
[6] Shu T, et al. SARS-Coronavirus-2 Nsp13 possesses NTPase and RNA helicase activities that can be inhibited by bismuth salts. *Virol Sinica.*. 2020:1.
[7] Borgio JF, et al. State-of-the-art tools unveil potent drug targets amongst clinically approved drugs to inhibit helicase in SARS-CoV-2. *Arch Med Sci AMS.* 2020;16(3):508.
[8] Khater S, Das G. Repurposing Ivermectin to inhibit the activity of SARS CoV2 helicase: possible implications for COVID 19 therapeutics. 2020.
[9] Chen J, et al. Structural basis for helicase-polymerase coupling in the SARS-CoV-2 replication-transcription complex. *Cell.*. 2020.
[10] Sethi A, et al. Molecular docking in modern drug discovery: Principles and recent applications. In: Drug Discovery and Development-New Advances. 2019, IntechOpen.
[11] Sreenivasulu C, et al. A simple Lewis acid induced reaction of phenols with electrophiles: synthesis of functionalized 4 H-chromenes and ortho-benzylphenols. *Synth Commun.* 2020;50(1):112–122.
[12] Huyut Z, Beydemir Ş, Gülçin İ. Antioxidant and antiradical properties of selected flavonoids and phenolic compounds. *Biochem Res Int.*. 2017.
[13] Pinto T, et al. Bioactive (Poly) phenols, volatile compounds from vegetables, medicinal and aromatic plants. *Foods.* 2021;10(1):106.
[14] Ercoli S, et al. Stability of phenolic compounds, antioxidant activity and colour parameters of a coloured extract obtained from coloured-flesh potatoes. *LWT.* 2021;136:110370.
[15] Trott O, Olson AJ. AutoDock Vina: improving the speed and accuracy of docking with a new scoring function, efficient optimization, and multithreading. *J Comput Chem.* 2010;31(2):455–461.
[16] Frisch M, et al. 309 Barone, V.; Petersson, G.; Nakatsuji, H., Gaussian 16. Revision A, 2016. 3, p. 310.
[17] Dennington R, Keith T, Millam J. GaussView, version 5. 2009.
[18] Burley SK, et al. Protein Data Bank (PDB): the single global macromolecular structure archive. *Protein Crystallogr.*. 2017:627–641.
[19] Dallakyan S. MGLTools. Reference Source, 2010.
[20] Visualizer DS. Biovia. Dassault Systèmes, BIOVIA Workbook, Release, 2020.
[21] Pires DE, Blundell TL, Ascher DB. pkCSM: predicting small-molecule pharmacokinetic and toxicity properties using graph-based signatures. *J Med Chem.* 2015;58(9):4066–4072.
[22] Cousins KR. Computer review of ChemDraw ultra 12.0. *J Am Chem Soc.* 2011;133(21):8388.
[23] Lu L, et al. Theoretical investigation on the antioxidative activity of anthocyanidins: A DFT/B3LYP study. *Dyes Pigm.* 2014;103:175–182.
[24] Shivaleela B, Hanagodimath S. UV-Visible Spectra, HOMO-LUMO Studies on Coumarin Derivative Using Gaussian Software.
[25] Gültekin Z, et al. A combined experimental (XRD, FT-IR, UV-VIS and NMR) and theoretical (NBO, NLO, local & global chemical activity) studies of methyl 2-((3R, 4R)-3-(naphthalen-1-yl)-4-(phenylsulfonyl) isoxazolidin-2-yl) acetate. *J Mol Struct.* 2020;1199:126970.
[26] Silvarajoo S, et al. Dataset of theoretical molecular electrostatic potential (MEP), highest occupied molecular orbital-lowest unoccupied molecular orbital (HOMO-LUMO) band gap and experimental cole-cole plot of 4-(ortho-, meta-and para-fluorophenyl) thiosemicarbazide isomers. *Data in Brief.*. 2020:106299.
[27] White MA, Lin W, Cheng X. Discovery of COVID-19 inhibitors targeting the SARS-CoV-2 Nsp13 helicase. *J Phys Chem Lett.* 2020;11:9144–9151.
[28] Gurung AB. In silico structure modelling of SARS-CoV-2 Nsp13 helicase and Nsp14 and repurposing of FDA approved antiviral drugs as dual inhibitors. *Gene Rep.* 2020;21:100860.
[29] Adedeji AO, Lazarus H. Biochemical characterization of Middle East respiratory syndrome coronavirus helicase. *mSphere.* 2016;1(5).
[30] Kousar K, et al. Phytochemicals from selective plants have promising potential against SARS-CoV-2: investigation and corroboration through molecular docking, MD simulations, and quantum computations. *Biomed Res Int.* 2020;2020.
[31] Maleki S, et al. Surface plasmon resonance, fluorescence, and molecular docking studies of bovine serum albumin interactions with natural coumarin diversin. *Spectrochim Acta Part A Mol Biomol Spectrosc.* 2020;230:118063.
[32] Design L. Pharmacophore and ligand-based design with. *Biovia Discovery Studio®.*. 2014.
[33] Best RB, et al. Optimization of the additive CHARMM all-atom protein force field targeting improved sampling of the backbone ϕ, ψ and side-chain χ1 and χ2 dihedral angles. *J Chem Theory Comput.* 2012;8(9):3257–3273.

[34] Phillips JC, et al. Scalable molecular dynamics on CPU and GPU architectures with NAMD. *J Chem Phys.* 2020;153(4):044130.
[35] Ding J, Arnold E. VMD. 2006.
[36] Kumar D, et al. Promising inhibitors of main protease of novel corona virus to prevent the spread of COVID-19 using docking and molecular dynamics simulation. *J Biomol Struct Dyn.*. 2020:1–15.
[37] Ahmad S, et al. Molecular docking, simulation and MM-PBSA studies of nigella sativa compounds: a computational quest to identify potential natural antiviral for COVID-19 treatment. *J Biomol Struct Dyn.*. 2020:1–9.
[38] Ishak SNH, et al. Molecular dynamic simulation of space and earth-grown crystal structures of thermostable T1 lipase Geobacillus zalihae revealed a better structure. *Molecules.* 2017;22(10):1574.
[39] Guan L, et al. ADMET-score–a comprehensive scoring function for evaluation of chemical drug-likeness. *Medchemcomm.* 2019;10(1):148–157.
[40] Chen X, et al. Analysis of the physicochemical properties of acaricides based on Lipinski's rule of five. *J Comput Biol.*. 2020.